Guide to Geophysical Data for the Northern Rocky Mountains and Adjacent Areas, Idaho, Montana, Washington, Oregon, and Wyoming

By Edward A. Mankinen[1], Thomas G. Hildenbrand[1], Michael L. Zientek[2], Stephen E. Box[2], Arthur A. Bookstrom[2], Mary H. Carlson[2], and Jeremy C. Larsen[2]

Open-File Report 2004–1413

2004

U.S. DEPARTMENT OF THE INTERIOR
U.S. GEOLOGICAL SURVEY

[1]USGS, 345 Middlefield Road, Menlo Park, California 94025
[2]USGS, 904 W. Riverside Avenue, Spokane, Washington 99201

TABLE OF CONTENTS

ILLUSTRATIONS

ABSTRACT

Geophysical (potential-field) data can provide an efficient means of delineating subsurface geology and structure over areas at varying scales. We are using regional aeromagnetic and gravity surveys, and their various derivative maps (e.g., Blakely, 1995; Hildenbrand and others, 2000), to investigate the geologic and tectonic framework of the Columbia–Missouri Rivers headwaters region (herein referred to as the study area), which encompasses the Northern High Plains and the Northern Rocky Mountains. The major focus of the project is to develop regional digital earth science data and interpretations that can be used by Federal land managers in regional planning and special assessments such as road-less area withdrawals. The study area encompasses all lands managed by the U.S. Forest Service (USFS) in Idaho north of the Snake River Plain and in western Montana. Geophysical techniques can delineate major crustal boundaries and deep crustal structures that may be localizing mineral deposits and controlling regional fluid flow. These techniques are particularly useful for investigating areas that are covered by thick, surficial deposits. Our purpose here is to describe, briefly, techniques to enhance particular anomaly characteristics (e.g., trend or wavelength), present the resulting maps, and suggest ways in which they may prove most useful. In-depth interpretations are deferred to subsequent publications.

INTRODUCTION

Gravity Data

The gravitational attraction at the Earth's surface can be modeled assuming a rotating, uniformly dense body. This gravity field, however, varies on a global scale because of effects due to Earth tides, differences in elevation, local topography, and variation in density of the subsurface. Fortunately, many of these variations can be predicted and are compensated to derive the "Bouguer anomaly" as described below. To remove the effects of isostatic roots to topographic loads at regional scales, a regional isostatic field is subtracted from the Bouguer gravity to produce an "isostatic residual gravity anomaly." The isostatic residual field enhances features that reflect local density variations in the middle and upper crust.

Gravity data for the study area were extracted from an unpublished dataset for the western United States compiled for the study by Hildenbrand and others (2000). This and similar compilations generally begin with the national gravity datasets compiled and maintained by the National Image and Mapping Agency (NIMA). An on-line, upgraded gravity database for the United States currently is also being developed by the Pan-American Center for Earth and Environmental Studies at the University of Texas, El Paso (http://paces.geo.utep.edu) as part of a collaborative effort with NIMA, the U.S. Geological

Survey (USGS), National Oceanic & Atmospheric Administration (NOAA), National Aeronautics and Space Administration (NASA), and National Science Foundation (NSF) (Keller and others, 2002; Hildenbrand and others, 2002a, 2002b).

Aeromagnetic Data

Aeromagnetic surveys are an efficient means of collecting a great amount of geophysical information over a broad area. The data, however, are difficult to interpret because the geomagnetic field is affected by both internal and external sources, and the magnetization of individual geologic bodies can be complex and variable over short distances, all of which make the magnetic field less predictive than the gravity field. Despite these complications, both external fields and those generated in the Earth's core can be generally well characterized, allowing the isolation of magnetic fields due to crustal sources (Blakely and Connard, 1989; Blakely, 1995). The anomalies remaining after removing the effects of short-period temporal activity resulting from external magnetic sources and subtracting the appropriate International Geomagnetic Reference Field (IGRF) represent the total magnetization (vector sum of both remanent and induced components) of rocks generally interpreted to lie above mid-crustal regions, or roughly at depths of 10-15 km (Jachens and others, 1989).

Aeromagnetic data analyzed in this report were obtained from the recently available, digital magnetic anomaly database and map for North America (North American Magnetic Anomaly Group [NAMAG], 2002). Because aeromagnetic survey specifications are often widely disparate, this latest map and database, resulting from a collaborative effort between the Geological Survey of Canada (GSC), the Consejo de Recursos Minerales de México (CRM), and the USGS, represents a major improvement over previously existing information. Data from Canada, Mexico, and the United States were reprocessed, gridded, converted from level to drape, and merged into a coherent representation of the data as if they had all been flown at a constant 305 m above terrain. Because wavelengths greater than about 150 km in the compilation are unreliable, due mainly to datum shifts between the merged surveys, a 500-km high-pass filter was used for correction (NAMAG, 2002).

ACKNOWLEDGMENTS

We thank Barry Moring for assistance with the grid conversions, and J. Glen and G. Phelps for constructive reviews of the manuscript and metadata.

METHODS

Gravity data for the western United States were obtained from a variety of sources in the form of scattered data. These data were then gridded by Hildenbrand and others (2000) at a spacing of 1 km using the minimum curvature algorithm of Webring (1982). Data for the study area were extracted from their compilation. The aeromagnetic data were extracted from the North American magnetic anomaly database (NAMAG, 2002), already gridded at a spacing of 1 km and available at http://pubs.usgs.gov/of/2002/ofr-02-0414. Both data sets were re-projected to an Albers equal-area projection; the central meridian is 114ºW, the latitude of projection origin is 41ºN, and the first and second parallels are 44º and 48º, respectively. The gravity and magnetic data also were enhanced in a number of ways, summarized below, in order to better characterize causative sources of their anomalies (also see Blakely, 1995). We used a match filter (Syberg, 1972) to isolate specific wavelengths within the data sets using the band-pass filtering algorithms of Phillips (1997). Standard USGS geophysical grids were converted to Arc grids using an ARC/INFO Macro subroutine (B.C. Moring and G.A. Phelps, USGS, written communication, 2001). Geophysical data described herein are available as ArcInfo, Geosoft, or standard USGS grids.

GRAVITY MAPS

Gravity observations for the study area are available from more than 60,000 gravity stations shown in figure 1. The distribution of stations is highly irregular, with sparse coverage often resulting from limited accessibility due to rough topography and land protection status (Wilderness areas). Conversely, dense coverage can also be seen in the vicinity of sedimentary basins, some mining districts, along highways and rivers, and specific study areas. Variations in the quality of the gravity data may be considerable because measurements were made by different observers, at different times, and with differing techniques and instrumentation. Errors can be introduced during gravity observations, and in the data reduction process by uncertainties in terrain correction, reduction density and, most commonly, in the estimation of station elevation. Errors in station elevation may range from tens of feet when using contour interpolation, to several feet at benchmark or spot elevations, and as little as a few centimeters when using differential GPS or other precise surveying techniques. Thus, errors on the order of 0.3 mGal or more could be expected from errors in station elevation alone in earlier surveys not employing GPS or related technology. Simpson and Jachens (1989) and Simpson and others (1986) estimate that, in a typical regional gravity survey, the combined errors produce anomaly values accurate to within 2 mGal. Standard gravity reduction methods, described briefly in sections below, may be found in various reference works such as Dobrin and Savit (1988) and Blakely (1995).

Bouguer Gravity

The field value observed at each gravity station shown in figure 1 is corrected by first removing the attraction of the reference ellipsoid and the effects due to Earth tides and rotation. Additional corrections account for differences in elevation between the gravity station and the geoid (the free-air correction), and density of the material between them (the Bouguer correction). The average density of the crust used for the latter correction is generally 2670 kg/m^3, which is the reduction density used in this report. The simple Bouguer correction is made assuming a uniformly thick slab having an infinite horizontal extent. A series of terrain corrections can then be applied (e.g., Spielman and Ponce, 1984; Plouff, 1977) to the simple Bouguer anomaly in order to remove the effects of topography in the vicinity of an individual gravity station. These terrain corrections, which remove the effects of topography out to a radius of 166.7 km from the gravity station, constitute the complete Bouguer correction. The complete Bouguer anomaly for the study area, shown in figure 2, was extracted from a grid (4-km spacing) for the western United States (R.W. Simpson, USGS, unpublished compilation, 1993) and re-gridded to a 1-km spacing.

Isostatic Residual Gravity

Bouguer gravity anomaly maps are commonly used to investigate geology and structure in the subsurface (Simpson and others, 1986). Over an area as large as the study area, however, large-amplitude, long-wavelength anomalies caused by deep crustal and upper mantle density distributions related to isostatically compensating roots of topographic loads often distort or mask anomalies produced by near-surface geologic bodies (Jachens and others, 1989). This effect can be seen in the strong inverse correlation between Bouguer gravity and elevation (compare figures 2 and 3). To remove the effects of the long-wavelength part of the gravity field, an isostatic regional field was calculated using an Airy-Heiskanen model (Heiskanen and Vening Meinesz, 1958) for local compensation of topographic loads (Simpson and others, 1983, 1986). The model assumes a crustal thickness of 25 km, a crustal density of 2670 kg/m^3, and a 400 kg/m^3 density contrast between the crust and mantle. Isostatic residual gravity values produced by subtracting the isostatic regional from the Bouguer anomaly generally contain errors less than 1 mGal, but locally the errors may be as much as 5 mGal (Simpson and others, 1986; Jachens and others, 1989). The isostatic residual gravity field for the study area, shown in figure 4, was extracted from the unpublished grid of isostatic residual gravity for the western United States (Hildenbrand and others, 2000). These anomalies are derived mainly from the gravity observations at the stations shown in figure 1 but, because this map is extracted from a larger grid, control along its margins is obtained from stations outside the study area.

Terraced Isostatic Residual Gravity. The terracing algorithm of Cordell and McCafferty (1989) was applied to the isostatic residual gravity and the resulting grid is shown in figure 5. The terracing function produces a field comprised of uniform domains separated by abrupt domain boundaries rather than the typical, smoothly varying gravity and magnetic contour maps. Terraced maps are thus considered to be more closely analogous to geologic maps.

Vertical Derivative. The first vertical derivative of the isostatic residual gravity grid of figure 4 was generated and is shown in figure 6. To produce the map shown in this figure, the data were upward continued 10 km to suppress short-wavelength noise generated by the derivative. The vertical derivative map emphasizes short-wavelength anomalies and is therefore useful for comparing gravity with mapped surficial geology and distinguishing changes between major domains. Applying the first vertical derivative is equivalent to a pseudomagnetic transform (Jachens and others, 1989), which facilitates comparison with aeromagnetic anomalies, some of which will be discussed briefly in a later section. Prominent in figure 6 are the gravity highs of the Snake River Plain, Wind River Range (Hurich and Smithson, 1982), and Archean basement rocks of Montana, and the gravity low delineating the Idaho batholith. Many additional features can be distinguished here, and in other derivative maps below, that will be discussed in greater detail in later reports.

Intermediate-wavelength data. We filtered the isostatic residual gravity field (figure 4) using the band-pass, match-filtering algorithms of Phillips (1997) to isolate prominent wavelengths in the data. We selected a three-layer model to isolate the depths of gravity anomaly sources in the study area dataset. The intermediate-wavelength data shown in figure 7 have been upward continued 5 km to minimize remaining high-frequency noise. These data typically highlight anomalies in the upper crust and serve to more clearly delineate some of the anomalies seen by the first vertical derivative. Examples here include the low-density material underlying the Yellowstone caldera, dense rocks of the Stillwater Complex and those along the NE-trending structures of the Great Falls Tectonic Zone (O'Neill and Lopez, 1985).

Long-wavelength data. Filtering to isolate long-wavelength data (figure 8) highlights, in general, anomalies due to mid-crustal sources and de-emphasizes shallow, thin sources and noise due to measurement errors. Although deep sources produce long-wavelength anomalies, shallow sources that are extensive over a wide area or extend to substantial depths may also produce some long wavelengths in addition to short wavelengths. Overall, however, long-wavelength isostatic residual gravity anomalies will provide insights as to the configuration and relationships of major geologic bodies generally within the upper 10-15 km of the crust (Jachens and others, 1989). Comparing figures 6 and 8 shows that many of the major domains apparent at the surface extend to considerable depths. Further delineation

of these deep density sources, used together with deep magnetic sources and available geologic information, will be used to determine the geologic and structural underpinnings of the study area.

Maximum horizontal gradients. Horizontal gradients were calculated for the long-wavelength gravity anomalies shown in figure 8 (e.g., Cordell, 1979; Blakely, 1995). When calculated for two-dimensional data grids, horizontal gradients will place narrow ridges over significant changes in gravity (figure 9). The method of Blakely and Simpson (1986) was used to calculate maximum values of these gradients, the locations of which tend to overlie the edges of causative bodies with abrupt, near-vertical contacts. For non-vertical contacts between geologic units of contrasting densities, maximum values of the horizontal gradients will be displaced down-dip and away from the edges of the body. The maxima in the long-wavelength gravity data (figure 9), along with a visual inspection of the gradient "ridges" containing them, were used to constrain major gravity lineaments, which are shown in figure 10.

Gravity Inversion

To first order, the isostatic residual gravity field (figure 4) reflects a pronounced contrast between dense pre-Cenozoic rocks and significantly less dense overlying strata. Because of this relationship, the gravity inversion method derived by Jachens and Moring (1990) can be used to separate the isostatic residual anomaly into pre-Cenozoic "basement" and younger basin fields. This method was used to calculate thickness of Cenozoic basin fill for the Basin and Range province (Saltus and Jachens, 1995). An expanded data set for the western U.S. (R.C. Jachens, USGS, written communication, 1995) includes parts of the study area, and the grid shown in figure 11 was extracted from this compilation. The grid has not been modified to include drill-hole data in the study area and should only be used qualitatively.

MAGNETIC MAPS

Aeromagnetic data for the study area are available from more than 130 individual surveys with widely varying flight specifications (figure 12). Boundaries of these surveys were generalized from the data indexes for aeromagnetic maps of Idaho (McCafferty and others, 1999), Montana (McCafferty and others, 1998), Oregon (C.W. Roberts, USGS, written communication, 2003), Washington (Finn and others, 1998), and Wyoming (Kucks and Hill, 2000). These disparate data sets have been processed to a common datum and merged into the 2002 magnetic anomaly map for North America. Magnetic anomalies over the study area (figure 13) reflect measured magnetic intensities relative to the International Geomagnetic Reference Field (IAGA, 1992).

Magnetic Residual

A magnetic residual (figure 14) was produced by analytically upward-continuing the observed anomalies (figure 13) 50 m (Hildenbrand, 1983) and subtracting the result from the original grid. By removing the contribution of deeper sources (accentuated by the upward continuation) the procedure emphasizes surface and near-surface magnetic sources. Although there is a persistent NS-EW grain that is probably an artifact of the aeromagnetic survey boundaries (compare with figure 12), many geologic units and domains are evident. Important tectonic features also can be distinguished that range from the very prominent NE-trending structures of the Great Falls tectonic zone (figure 14) to the more subtle NW-trending strands of the Lewis and Clark line (e.g., Harrison and others, 1974).

Magnetic Potential

The aeromagnetic data of the study area were analyzed further by first transforming them to their magnetic potential (the "pseudogravity" transform – see, Baranov, 1957; Blakely, 1995) shown in figure 15. This procedure helps to isolate broad magnetic features that may be masked by high-amplitude shallow magnetic sources. Because the pseudogravity transform converts a magnetic anomaly into one that would be observed if the magnetic distribution of the body were replaced by an identical density distribution, interpretation of their sources is simplified by allowing the use of gravity techniques as described above.

Terraced Magnetic Potential. The terracing algorithm of Cordell and McCafferty (1989) was applied to the pseudogravity grid and the result is shown in figure 16.

Intermediate-wavelength data. The magnetic potential was filtered, using matched bandpass filtering (Phillips, 1997), to isolate the dominant wavelengths within the data set. The intermediate-wavelength data shown in figure 17 highlight magnetic sources in the upper crust. This grid emphasizes many of the same sources seen in the magnetic residual (figure 14) but removes much of the short-wavelength noise. Among the many features apparent here are the compositional zones comprising the Boulder batholith (Klepper and others, 1971).

Long-wavelength data. As with the gravity data, the long-wavelength data (figure 18) highlight anomalies due to mid-crustal sources and de-emphasizes shallow, thin sources although there may again be some contribution from wide-spread shallow sources. Long-wavelength magnetic data could represent sources lying somewhat above those indicated by the gravity data depending upon depth to the Curie-temperature isotherm. This isotherm, the temperature below which rocks do not retain their magnetic properties (above ~550°C), is typically located 20–25 km below the Earth's surface except in areas of high heat flow.

Maximum horizontal gradients. Because the aeromagnetic data were first transformed to their magnetic potential, the steepest horizontal gradients will reflect lateral changes in magnetization (e.g., Cordell and Grauch, 1985; Blakely, 1995). Horizontal gradients of the long-wavelength anomalies (figure 19) and their maxima were calculated (Blakely and Simpson, 1986) and used to constrain major lineaments in magnetic data (figure 20). A possible indication of shallow sources contributing to the long-wavelength data may be the northwest-trending lineaments in northwestern Montana (figure 20) that seem to be reflected also in the magnetic residual (figure 14) and intermediate-wavelength data (figure 17). These lineaments correspond closely to the outcrop pattern of the Burke and Revett Formations, both of which contain significant magnetite concentrations due to diagenetic alteration (e.g., Hayes, 1990).

CONCLUSIONS

The various geophysical grids described herein are useful for delineating deep-seated crustal structures that may be controlling regional fluid flow and thus localizing mineral deposits (see Hildenbrand and others (2000) for a thorough discussion). Bandpass-filtered gravity and magnetic potential data sets are useful for highlighting causative sources occurring at various levels within the crust. For example, many isolated circular anomalies are delineated by maxima in the horizontal gradients (figures 10 and 20). Some of these are particularly well-expressed by the magnetic residual (figure 14) which emphasizes surface and near-surface magnetic sources. Many of these maxima outline plutons exposed at the surface (Zientek and others, unpublished data, 2004), raising the possibility that other similar anomalies represent buried plutons which may be potential targets for undiscovered porphyry and vein deposits. Geophysical lineaments produced by the deep gravity and magnetic sources can be used as aids in determining major tectonic domains of the study area. Shallow structures such as mapped faults can be seen, as well as their continuation beneath areas covered by thick surficial deposits. Combining this information with mapped geology may aid in predicting the stability of landforms in certain areas under increased logging and mining activities. Landform stability, in turn, will help determine the health of ecosystems including, for example, salmon habitat and endangered species. Finally, extraction of data from specific areas within the study area can aid in smaller scale studies such as potential-field modeling of the Stillwater Complex (Mankinen, Hildenbrand, and Zientek, unpublished data, 2004).

REFERENCES

Baranov, V., 1957, A new method for interpretation of aeromagnetic maps: Pseudo-gravimetric anomalies: Geophysics, v. 22, p. 359-383.

Blakely, R.J., 1995, *Potential Theory in Gravity and Magnetic Applications*: New York, Cambridge University Press, 441 p.

Blakely, R.J., and Connard, G.G., 1989, Crustal studies using magnetic data, *in* Pakiser, L.C., and Mooney, W.D., eds., Geophysical Framework of the Continental United States: Geological Society of America Memoir 172, p. 45-60.

Blakely, R.J., and Simpson, R.W. 1986, Approximating edges of source bodies from magnetic or gravity anomalies: Geophysics, v. 51, p. 1494-1498.

Cordell, L., 1979, Gravimetric expression of graben faulting in Santa Fe County and the Española Basin, *in* Ingersoll, R.V., ed., Guidebook to Santa Fe County, 30th Field Conference: New Mexico Geological Society, p. 59-64.

Cordell, L., and Grauch, V.J.S, 1985, Mapping basement magnetization zones from aeromagnetic data in the San Juan Basin, New Mexico, *in* Hinze, W.J., ed., the utility of regional Gravity and Magnetic Anomaly Maps: Society of Exploration Geophysicists, Tulsa, Oklahoma, p. 181-197.

Cordell, L., and McCafferty, A.E., 1989, A terracing operator for physical property mapping with potential field data: Geophysics, v. 54, p. 621-634.

Dobrin, M.B., and Savit, C.H., 1988, *Introduction to Geophysical Prospecting* (4th ed.): New York, McGraw-Hill, 867 p.

Finn, C., Brenner, K.C., McCafferty, A., and Kuck, R., 1998, Washington aeromagnetic maps and data: U.S. Geological Survey Open-File Report 98-241.

Harrison, J.E., Griggs, A.B., and Wells, J.D., 1974, Tectonic features of the Precambrian Belt Basin and their influence on post-Belt structures: U.S. Geological Survey Professional Paper 866, 15 p.

Hayes, T.S., 1990, A preliminary study of thermometry and metal sources of the Spar Lake strata-bound copper-silver deposit, Belt Supergroup, Montana: U.S. Geological Survey Open-File Report 90-0484, 30 p.

Heiskanen, W.A., and Vening Meinesz, F.A., 1958, *The Earth and its gravity field*: New York, McGraw-Hill, 470 p.

Hildenbrand, T.G., 1983, FFTFIL: A filtering program based on two-dimensional Fourier analysis: U.S. Geological Survey Open-File Report 83-237, 61 p.

Hildenbrand, T.G., Berger, B., Jachens, R.C., and Ludington, S., 2000, Regional crustal structures and their relationship to the distribution of ore deposits in the western United States, based on magnetic and gravity data: Economic Geology, v. 95, p. 1583-1603.

Hildenbrand, T.G., Briesacher, A., Hinze, W., Hittelman, A., Keller, G.R., Kucks, R., Smith, D., and Roest, W., 2002a, Web-based U.S. gravity data system planned: Eos, Transactions of the American Geophysical Union, v. 83, no. 52, p. 613 and 618.

Hildenbrand, T.G., Briesacher, A., Flanagan, G., Hinze, W.J., Hittelman, A.M., Keller, G.R., Kucks, R.P, Plouff, D., Roest, W., Seeley, J., Smith, D.A., and Webring, M., 2002b, Rationale and operational plan to upgrade the U.S. gravity database: U.S. Geological Survey Open-File Report 02-463, 12 p.

Hurich, C.A., and Smithson, S.B., 1982, Gravity interpretation of the southern Wind River Mountains, Wyoming: Geophysics, v. 47, p. 1550-1561.

IAGA, Division V, Working Group 8, 1992, International geomagnetic reference field, 1991 revision, in Langel, R.A., Chairman, Analysis of the main field and secular variation: Geophysics, v. 57, p. 956-959.

Jachens, R.C., and Moring, B.C., 1990, Maps of the thickness of Cenozoic deposits and the isostatic residual gravity over basement for Nevada: U.S. Geological Survey Open-File Report 90-404, 15 p.

Jachens, R.C., Simpson, R.W., Blakely, R.J., and Saltus, R.W., 1989, Isostatic residual gravity and crustal geology of the United States, *in* Pakiser, L.C., and Mooney, W.D., eds., Geophysical Framework of the Continental United States: Geological Society of America Memoir 172, p. 405-424.

Keller, G.R., Hildenbrand, T.G., Kucks, R., Roman, D., and Hittelman, A.M., 2002, Upgraded gravity anomaly base of the United States: The Leading Edge (Tulsa, OK), v. 21, pp. 366-367, 387.

Klepper, M.R., Robinson, G.D., and Smedes, H.W., 1971, On the nature of the Boulder Batholith of Montana: Geological Society of America Bulletin, v. 82, p. 1563-1580.

Kucks, R.P., and Hill, P.L., 2000, Wyoming aeromagnetic and gravity maps and data: A web site for distribution of data: U.S. Geological Survey Open-File Report 00-0198.

McCafferty, A., Bankey, V., and Brenner, K.C., 1998, Montana aeromagnetic and gravity maps and data: U.S. Geological Survey Open-File Report 98-333.

McCafferty, A., Kucks, R.P., Hill, P.L., and Racey, S.D., 1999, Aeromagnetic map for the state of Idaho: A web site for distribution of data: U.S. Geological Survey Open-File Report 99-371.

North American Magnetic Anomaly Group (NAMAG), 2002, Digital data grids for the magnetic anomaly map of North America: U.S. Geological Survey Open-File Report 02-414, 4 p.

O'Neill, J.M., and Lopez, D.A., 1985, Character and regional significance of Great Falls Tectonic Zone, east-central Idaho and west-central Montana: American Association of Petroleum Geologists Bulletin, v. 69, p. 437-447.

Phillips, J.D., 1997, Potential-field geophysical software for the PC, version 2.2: U.S. Geological Survey Open-File Report 97-725, 34 p.

Plouff, D., 1977, Preliminary documentation for a FORTRAN program to compute gravity terrain corrections based on topography digitized on a geographic grid: U.S. Geological Survey Open-File Report 77-535, 45 p.

Saltus, R.W., and Jachens, R.C., 1995, Gravity and basin-depth maps of the Basin and Range province, western United States: U.S. Geological Survey Geophysical Investigations Map GP-1012, scale 1:2,500,000.

Simpson, R.W., and Jachens, R.C., 1989, Gravity methods in regional studies, *in* Pakiser, L.C., and Mooney, W.D., eds., Geophysical Framework of the Continental United States: Geological Society of America Memoir 172, p. 35-44.

Simpson, R.W., Jachens, R.C., and Blakely, R.J., 1983, Airyroot: a FORTRAN program for calculating the gravitational attraction of an Airy isostatic root out to 166.7 km: U.S. Geological Survey Open-File Report 83-883, 66 p.

Simpson, R.W., Jachens, R.C., Blakely, R.J., and Saltus, R.W., 1986, A new isostatic residual gravity map of the conterminous United States with a discussion on the significance of isostatic residual anomalies: Journal of Geophysical Research, v. 91, p. 8348-8372.

Spielman, J.B., and Ponce, D.A., 1984, HANDTC, a FORTRAN program to calculate inner-zone terrain corrections: U.S. Geological Survey Open-File Report 84-777, 20 p.

Syberg, F.J.R., 1972, A Fourier method for the regional-residual problem of potential fields: Geophysical Prospecting, v. 20, p. 47-75.

Webring, M., 1982, MINC–A gridding program based on minimum curvature: U.S. Geological Survey Open-File Report 81-1224, 43 p.

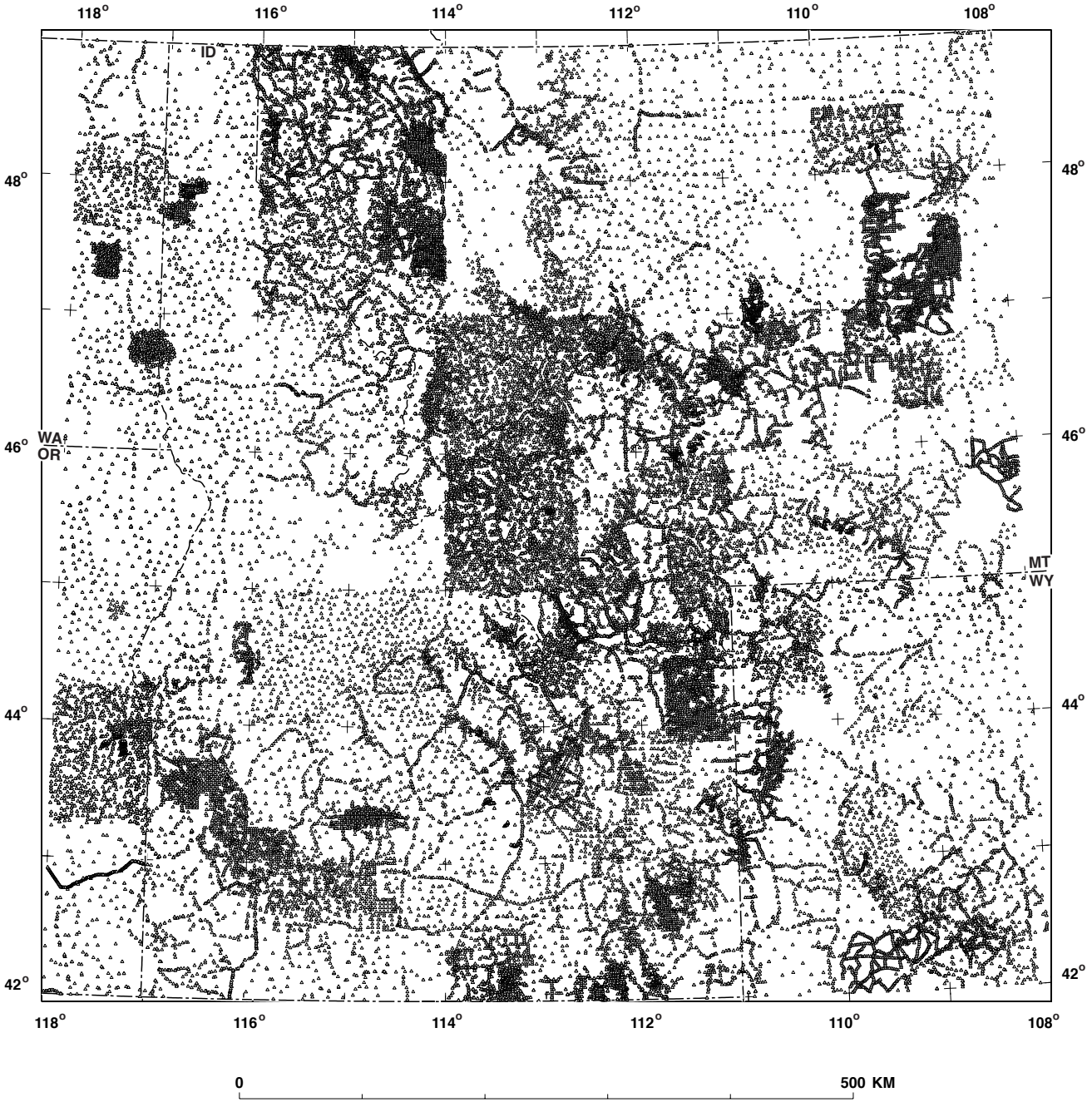

Figure 1. Gravity stations (triangles) within the study area.

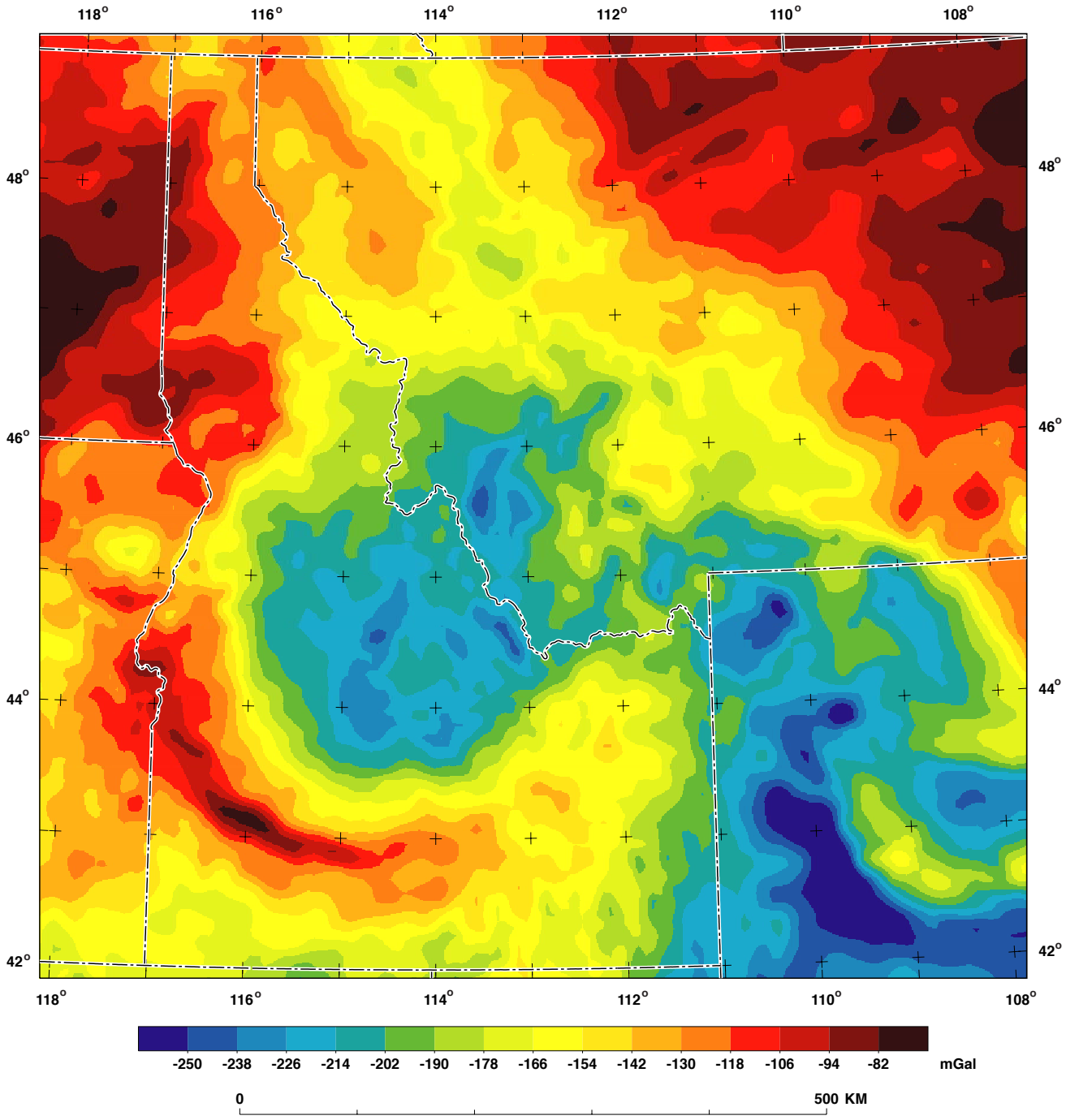

Figure 2. Complete Bouguer anomaly map of the study area. Extracted from a grid for the western United States (R.W. Simpson, unpublished data, 1993).

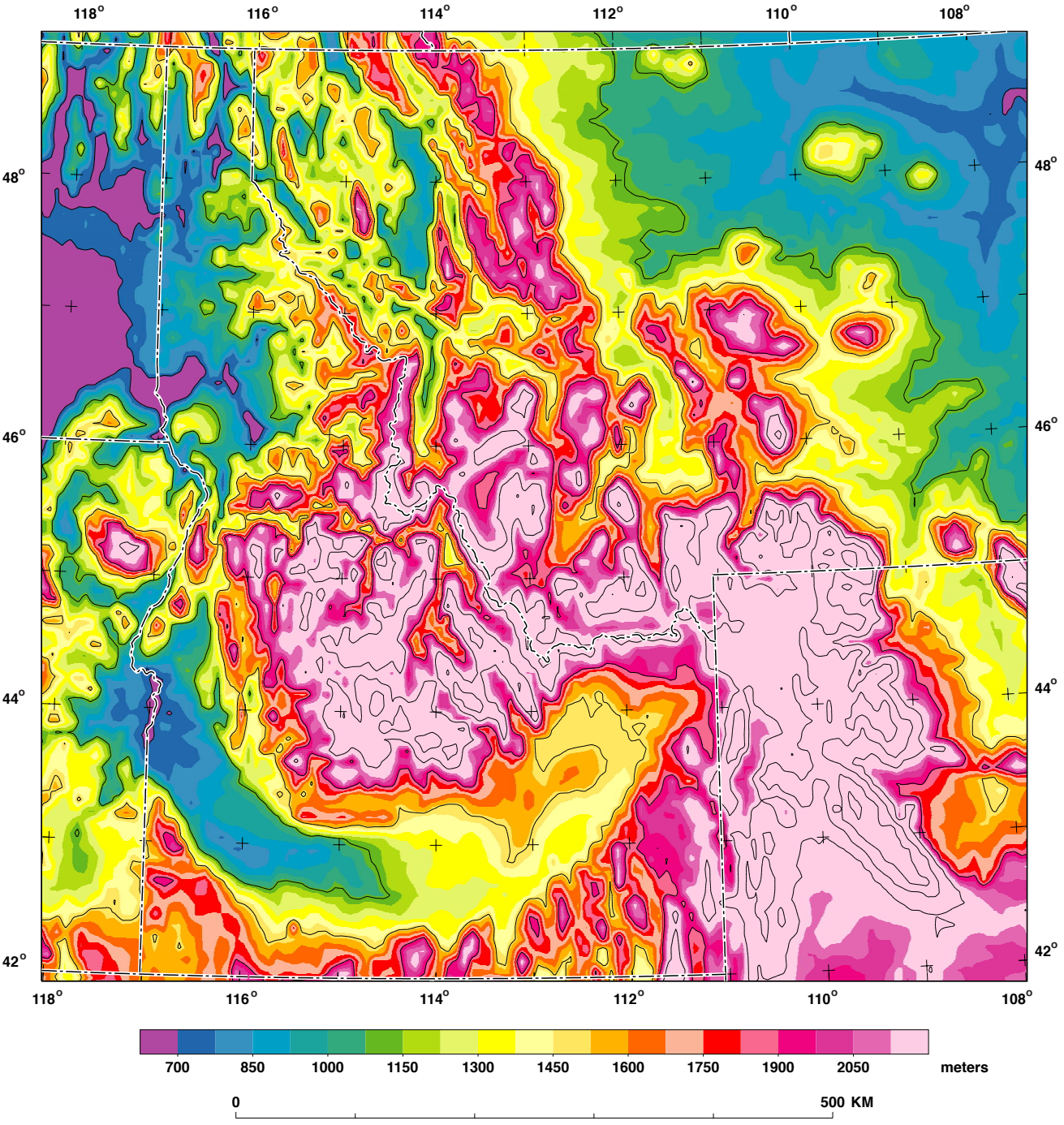

Figure 3. Topography (5-min grid) of the study area. Contour interval = 400m.

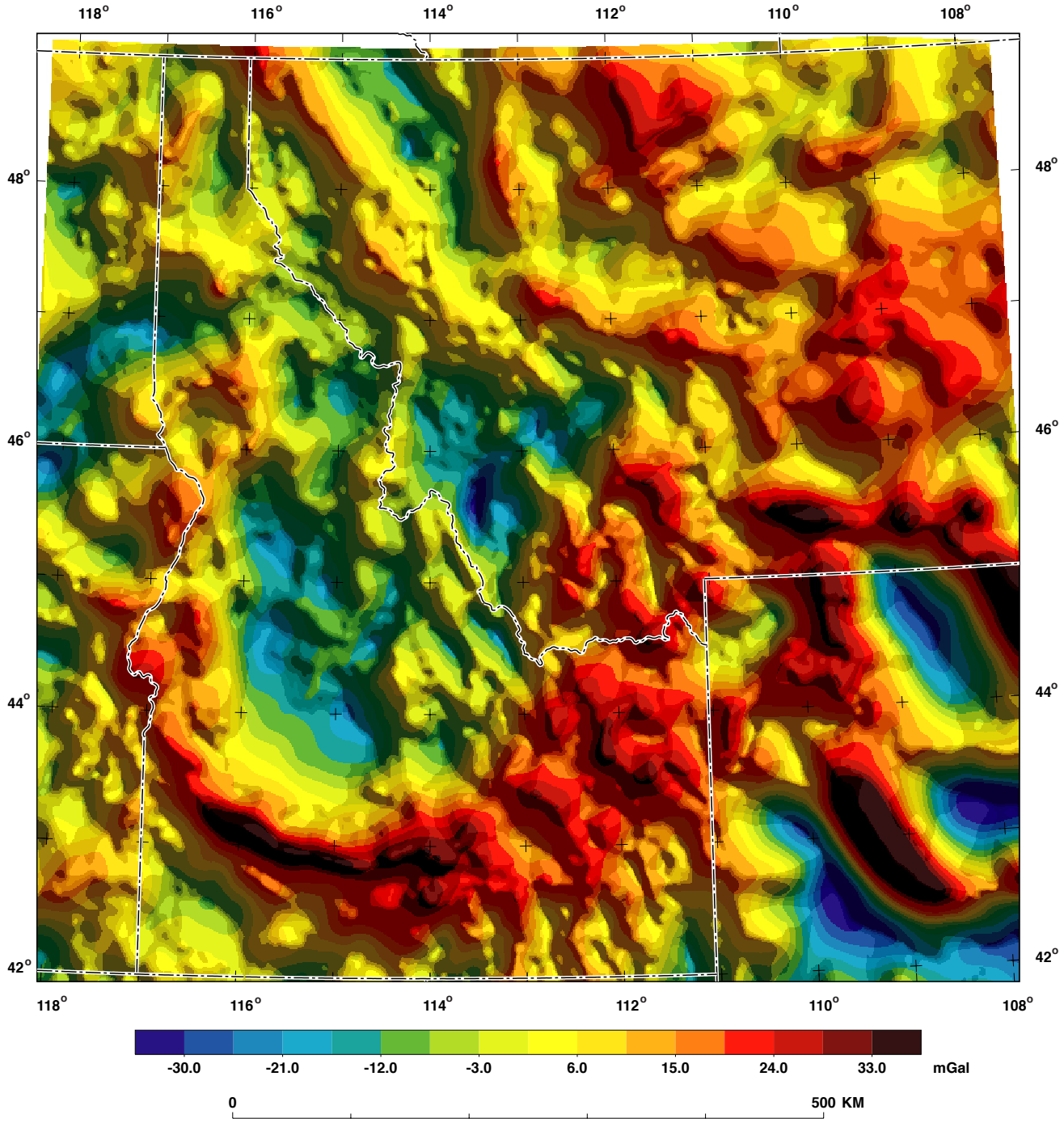

Figure 4. Isostatic residual gravity anomalies in the study area. Data upward continued 5 km to enhance regional aspects of the dataset. Extracted from an unpublished grid for the western United States (Hildenbrand and others, 2000).

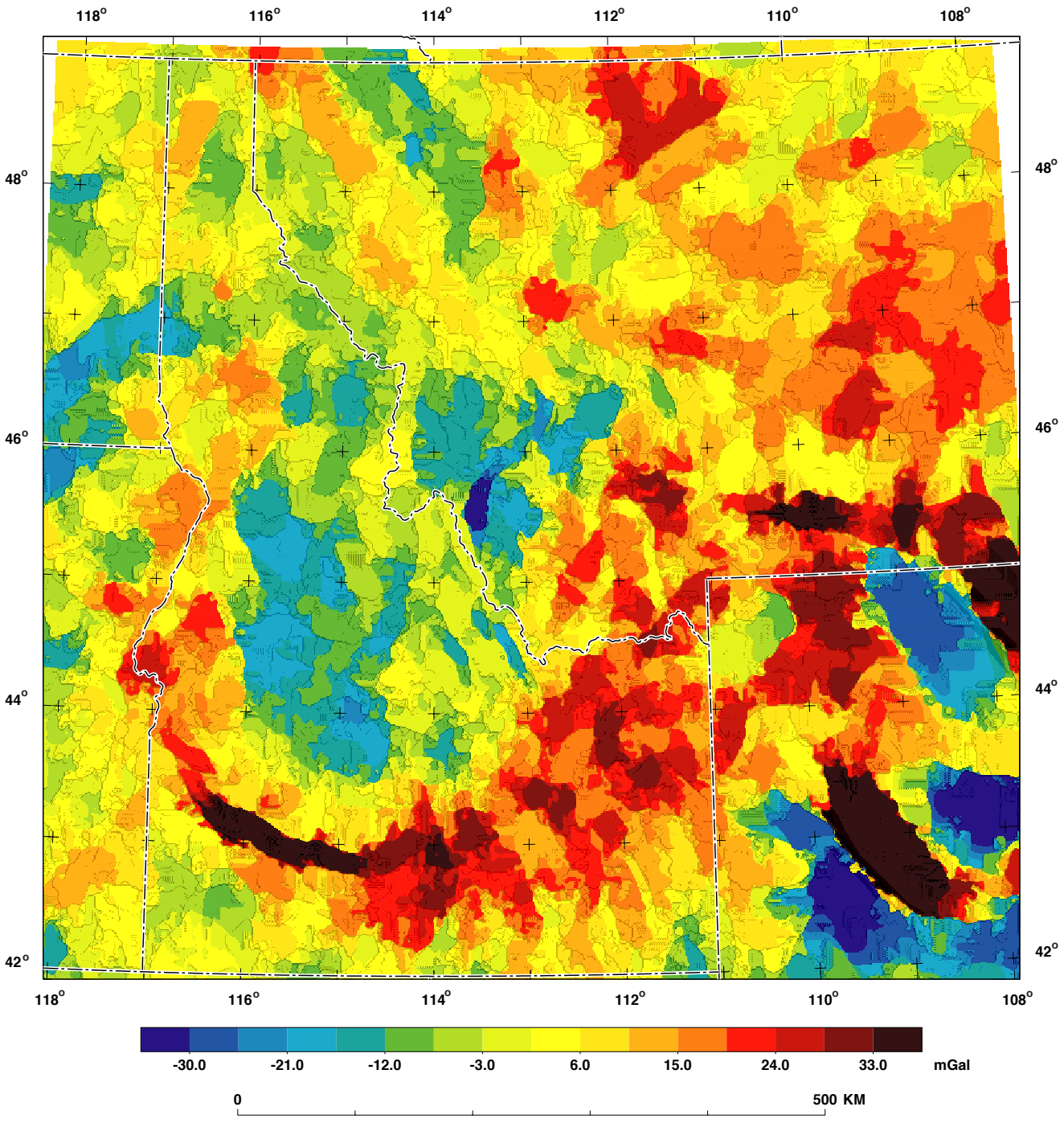

Figure 5. Terraced isostatic residual gravity using the method of Cordell and McCafferty (1989).

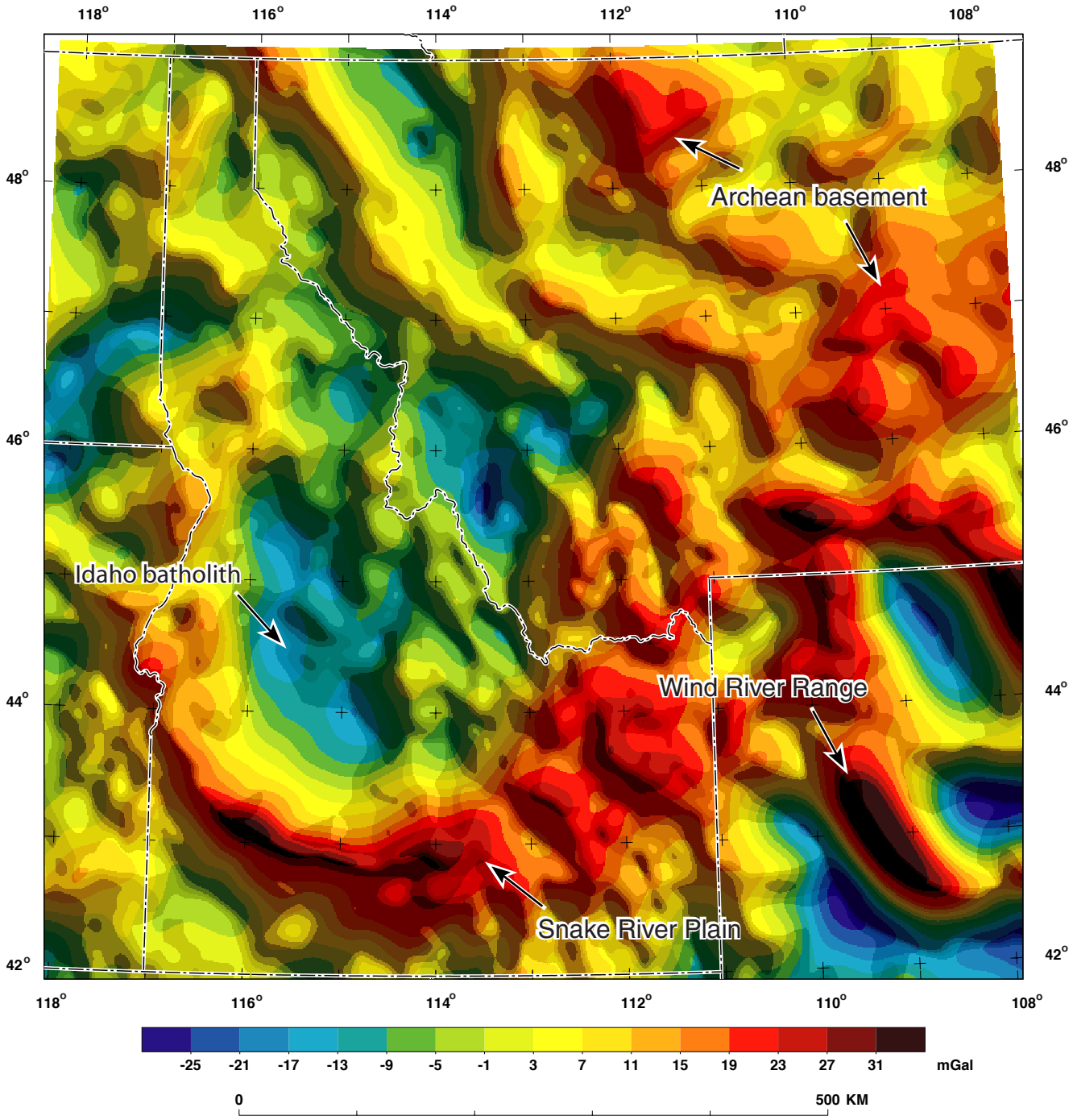

Figure 6. First vertical derivative of the isostatic residual gravity. Upward continued 10 km.

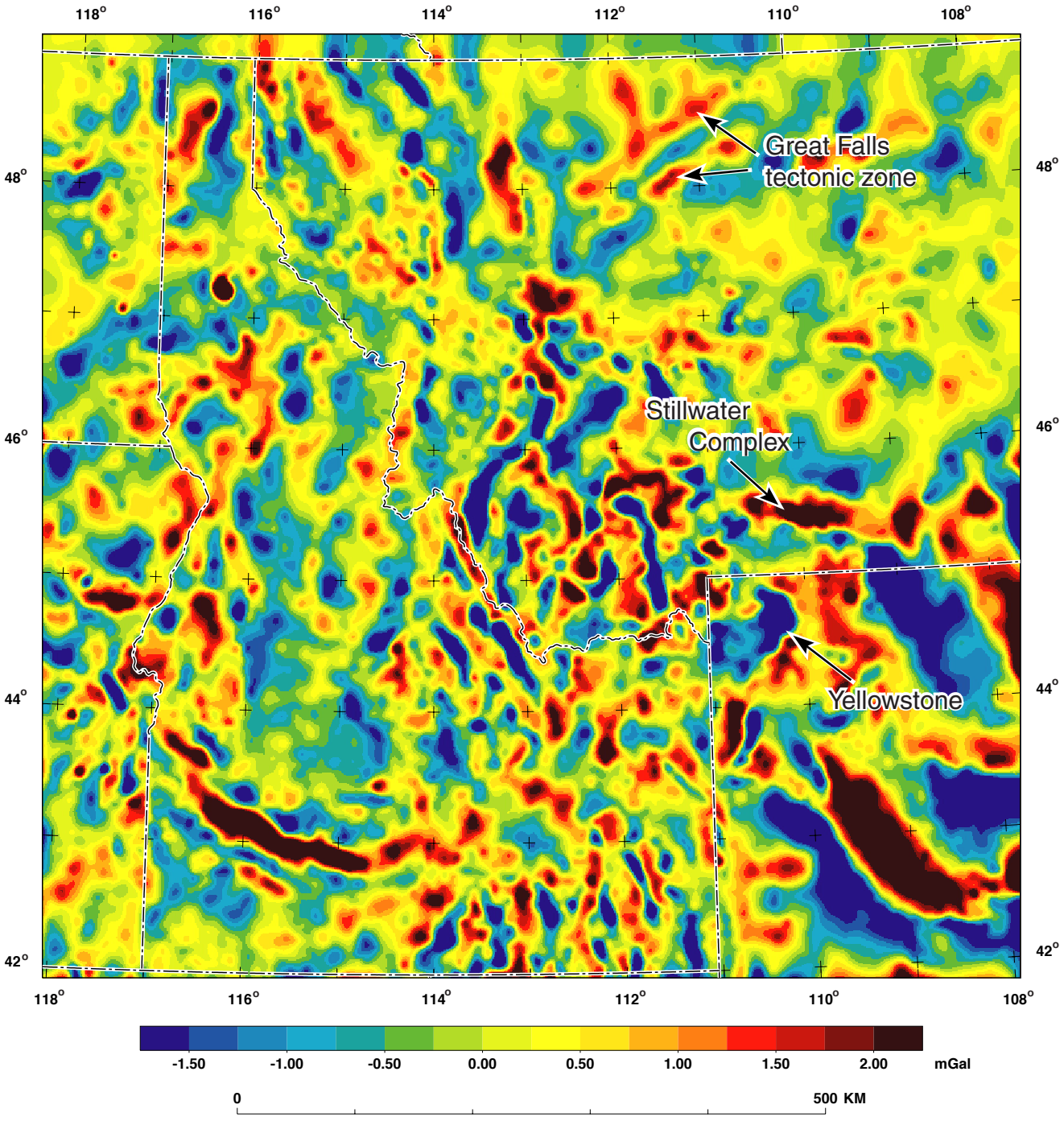

Figure 7. Intermediate-wavelength isostatic residual gravity, upward continued 5 km. A matched filter was applied to the isostatic residual gravity of figure 4 to enhance sources in the upper crust.

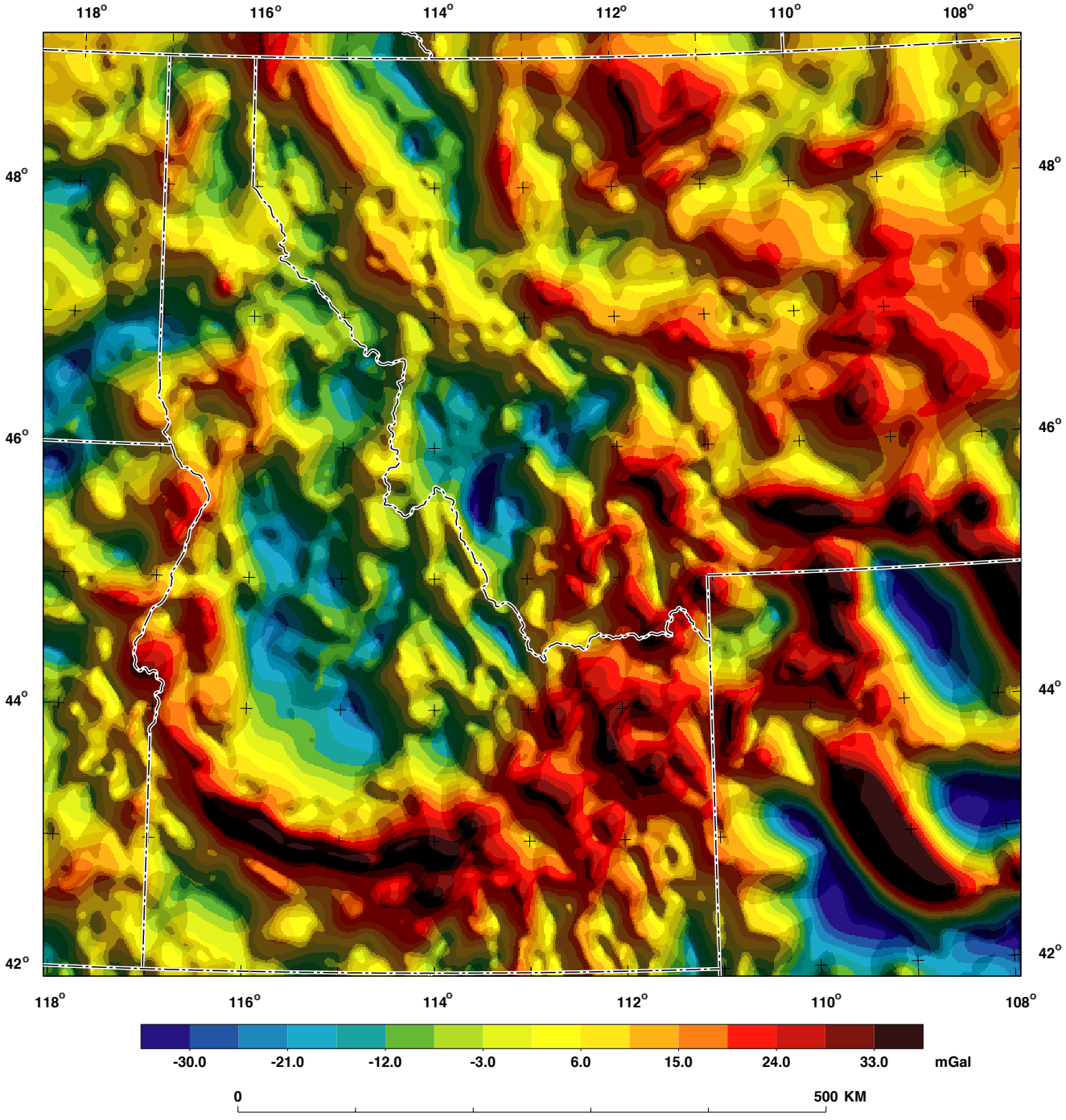

Figure 8. Long-wavelength isostatic residual gravity. A matched filter was applied to the isostatic residual gravity of figure 4 to enhance sources in the middle to upper crust.

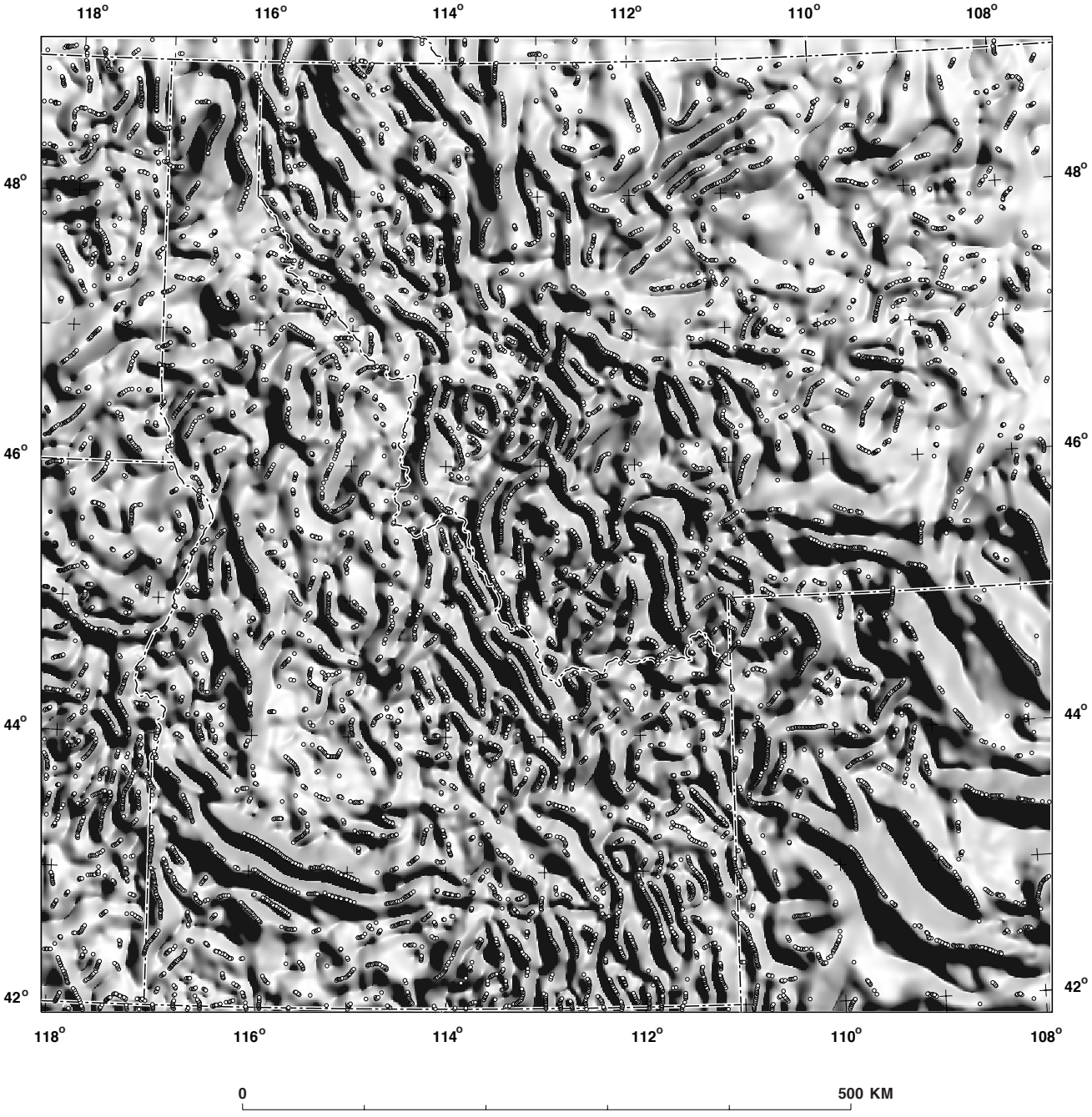

Figure 9. Shaded-relief map of horizontal gradients in the long-wavelength data shown in figure 8. Open circles are maximum values of these gradients calculated using the method of Blakely and Simpson (1986).

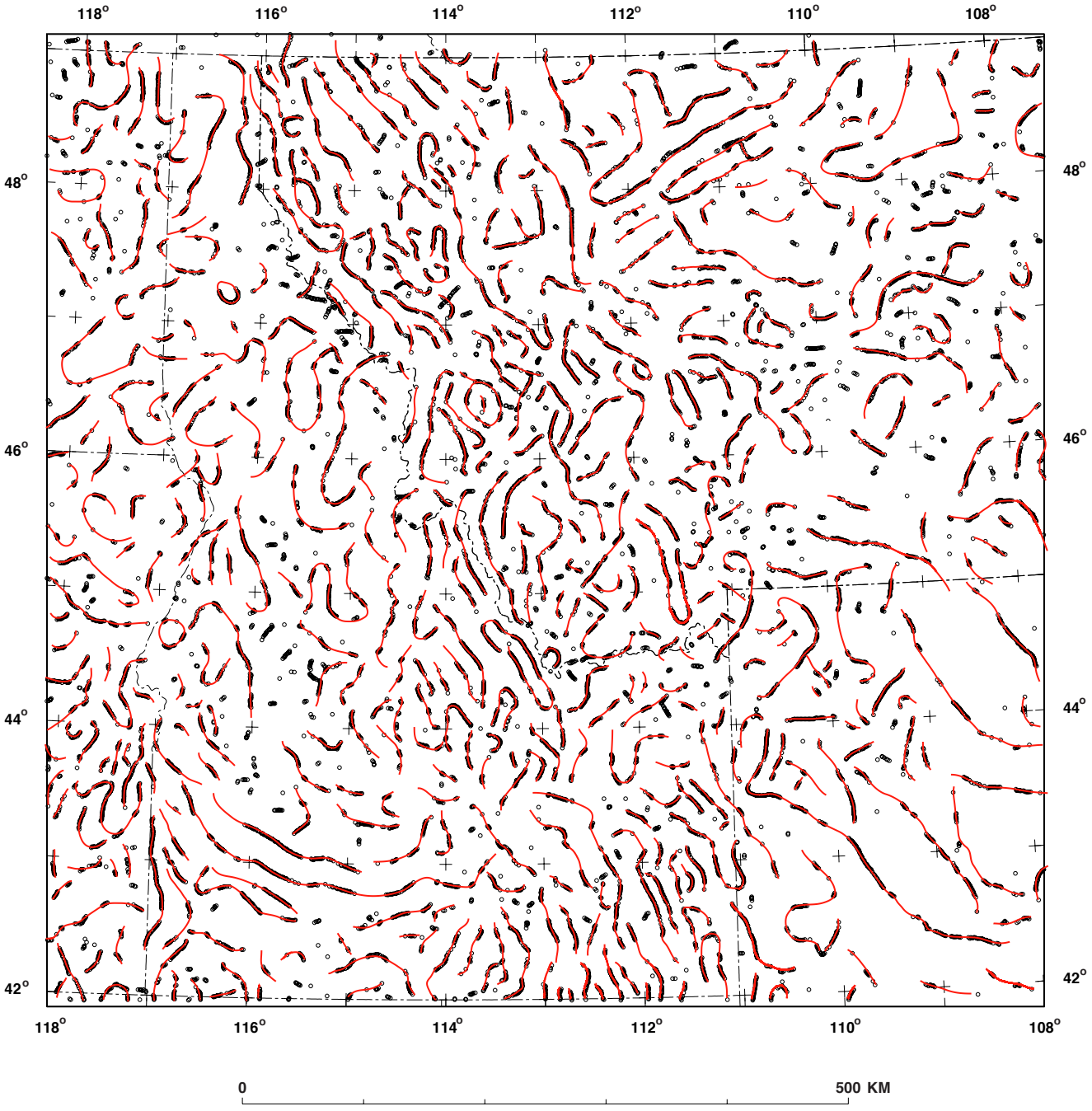

Figure 10. Interpreted major density boundaries (red lines) within the middle to upper crust constrained by maxima in the horizontal gradients shown in figure 9.

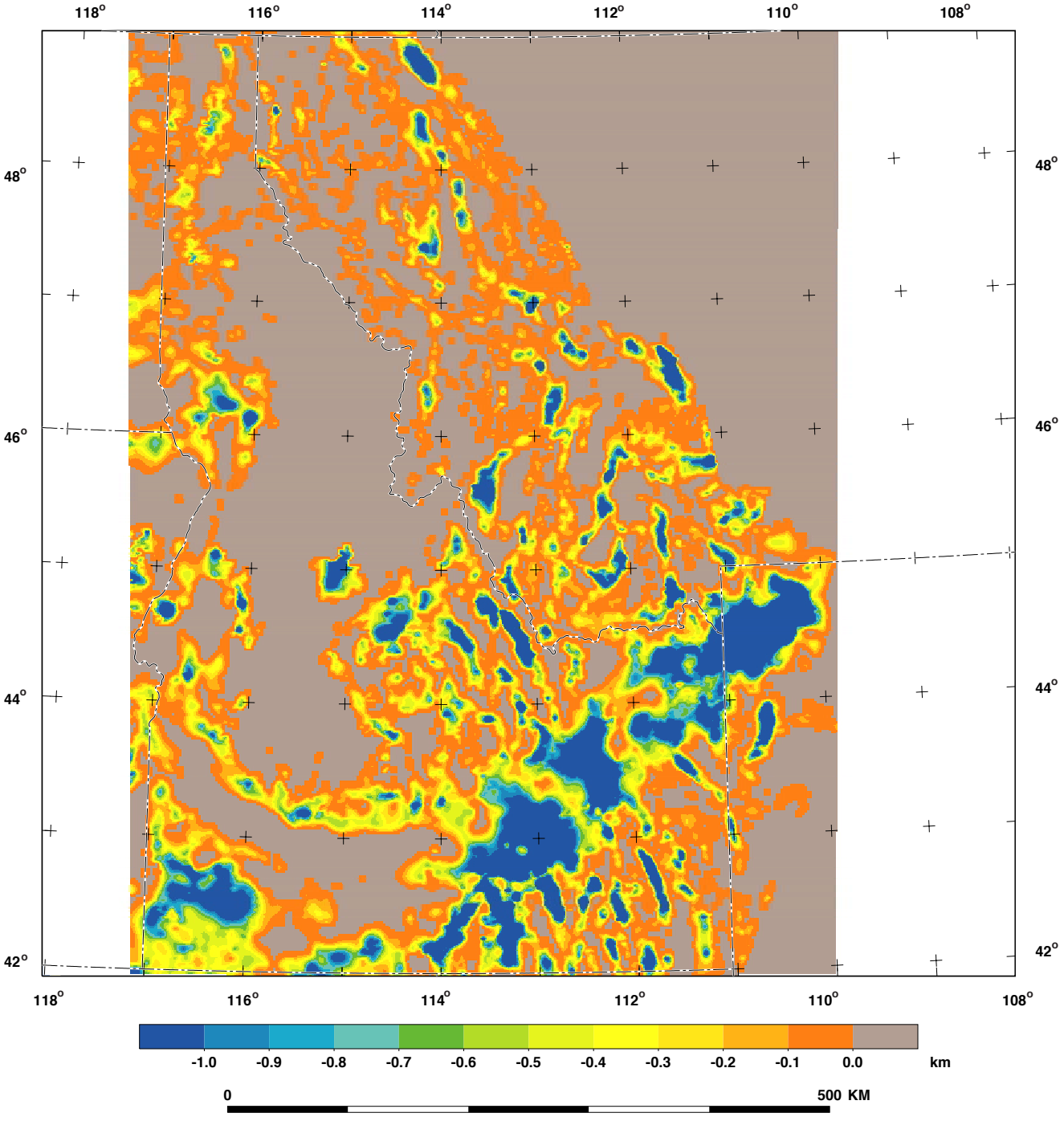

Figure 11. Depth to pre-Cenozoic basement as determined by the gravity inversion method of Jachens and Moring (1990). From R.C. Jachens, USGS, unpublished data, 1995.

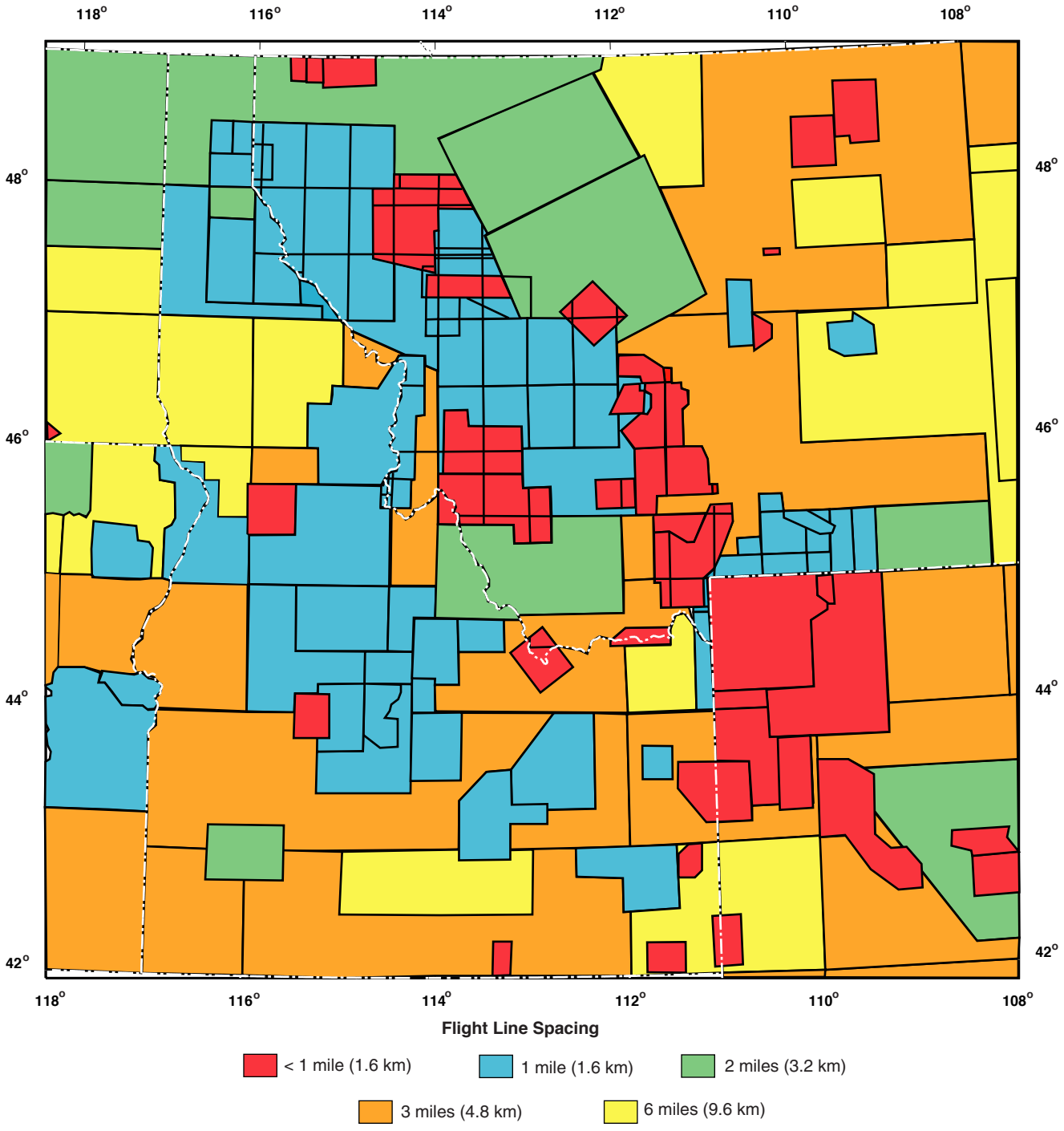

Figure 12. Generalized aeromagnetic survey boundaries of the study area.

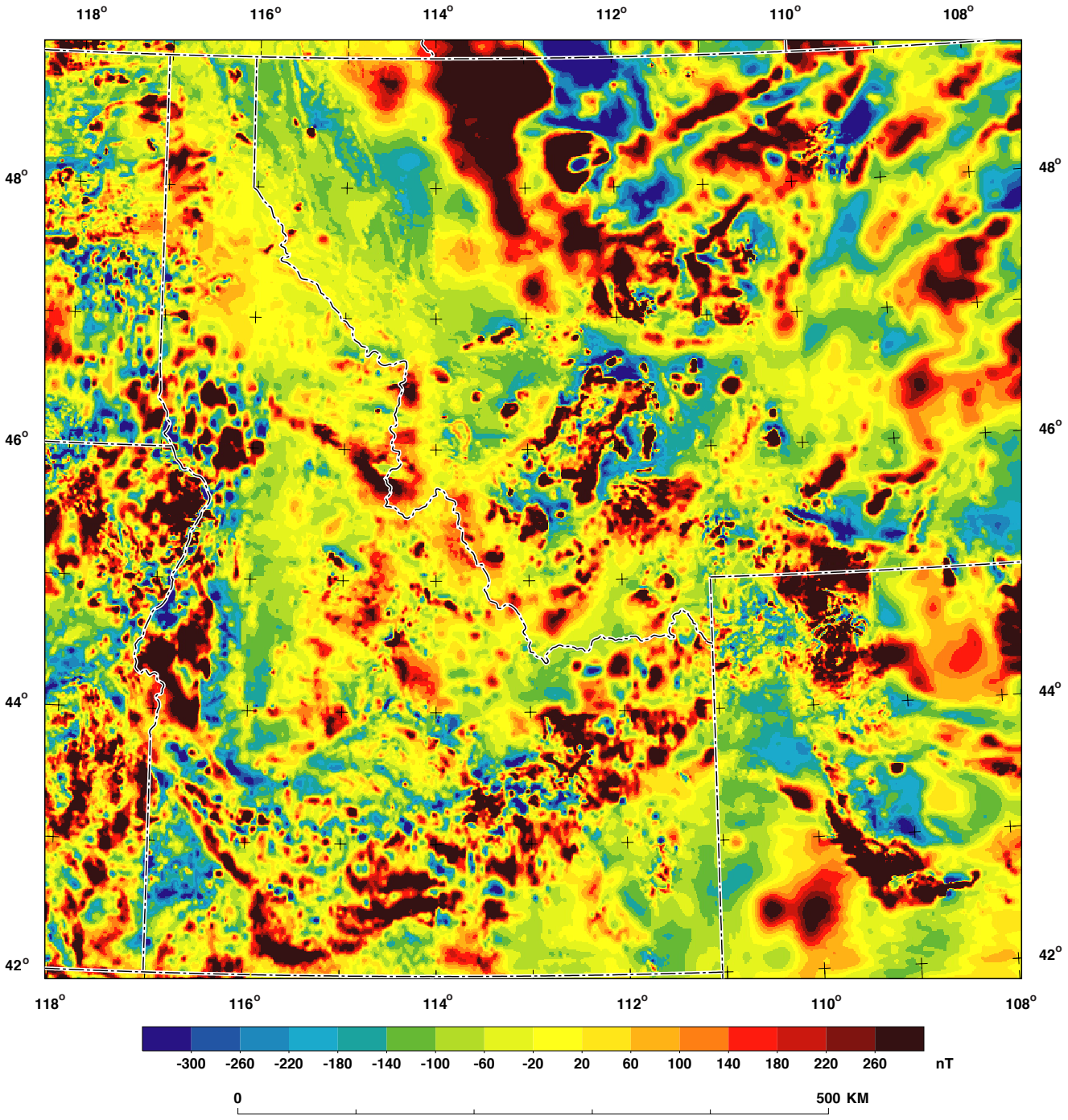

Figure 13. Aeromagnetic map of the study area, extracted from the Magnetic Anomaly Map of North America (NAMAG, 2002). Colors represent measured magnetic intensities relative to the International Geomagnetic Reference Field (IAGA, 1992).

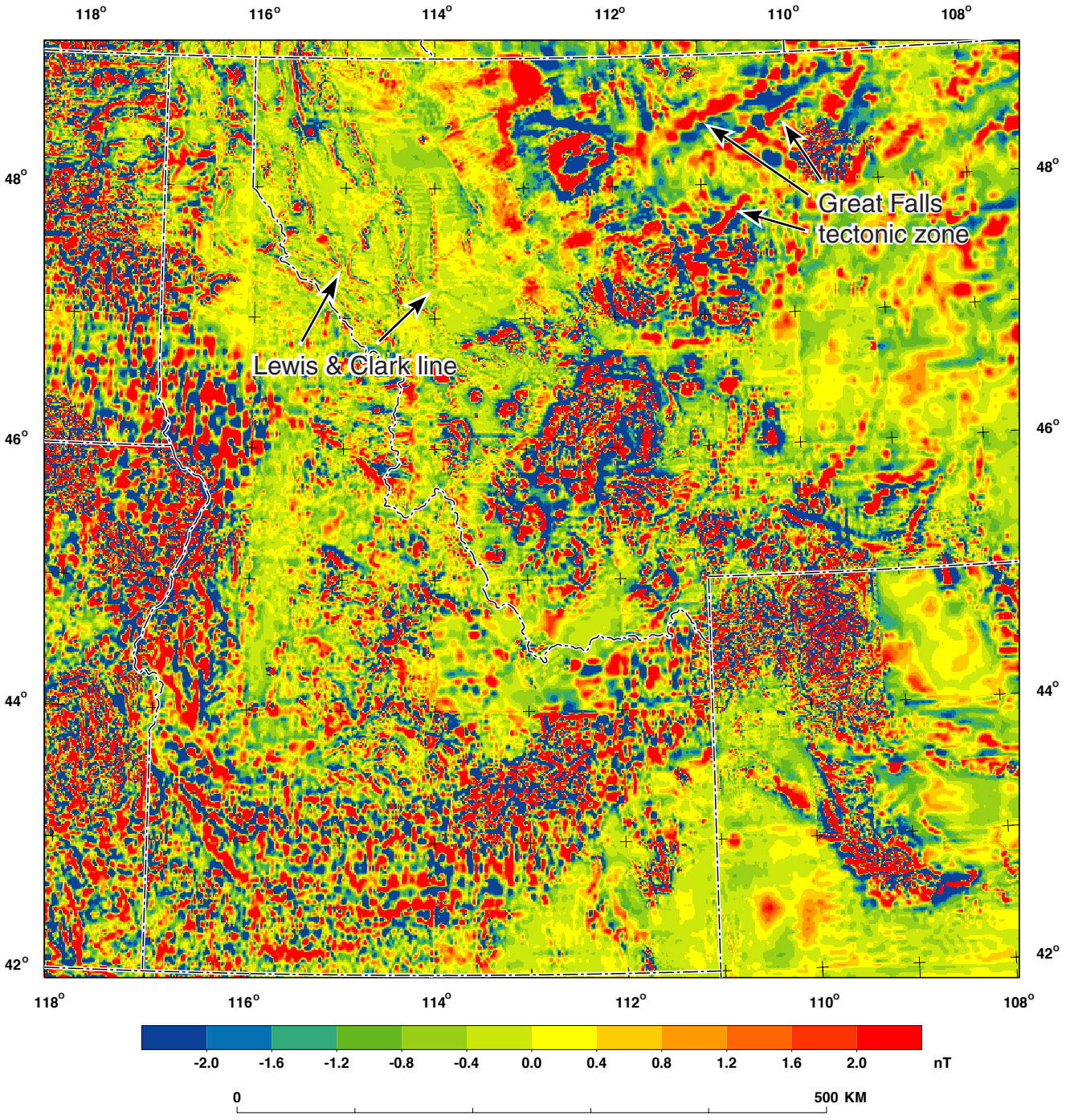

Figure 14. Residual magnetic anomalies calculated by analytically upward-continuing the observed anomalies (shown in figure 13) 50 m and subtracting the resulting grid from the original anomalies. This procedure enhances surface and near-surface magnetic sources.

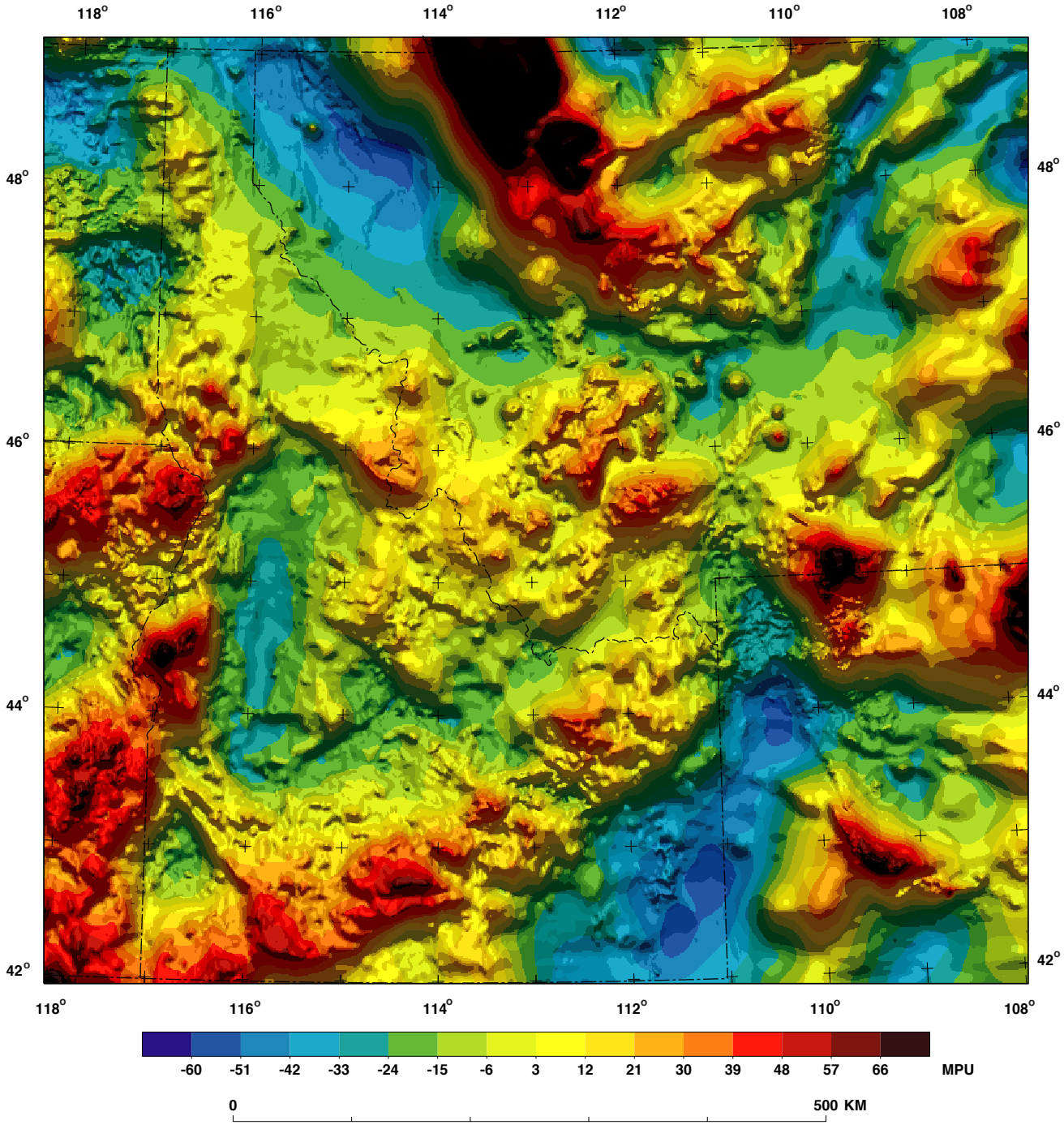

Figure 15. Aeromagnetic data of figure 13 transformed to their magnetic potential (the "pseudogravity" transform of Baranov, 1957).

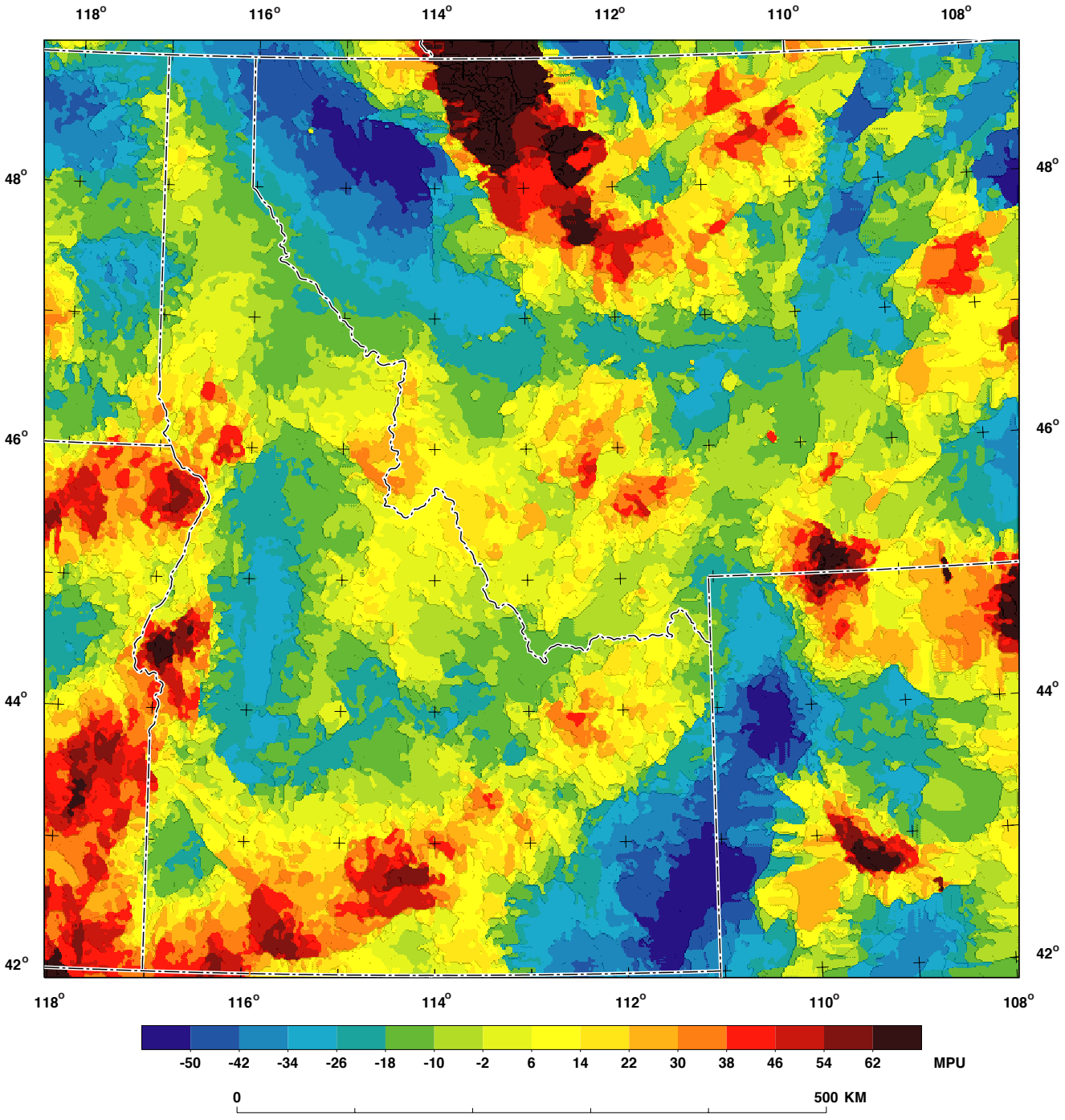

Figure 16. Terraced magnetic potential using the method of Cordell and McCafferty (1989).

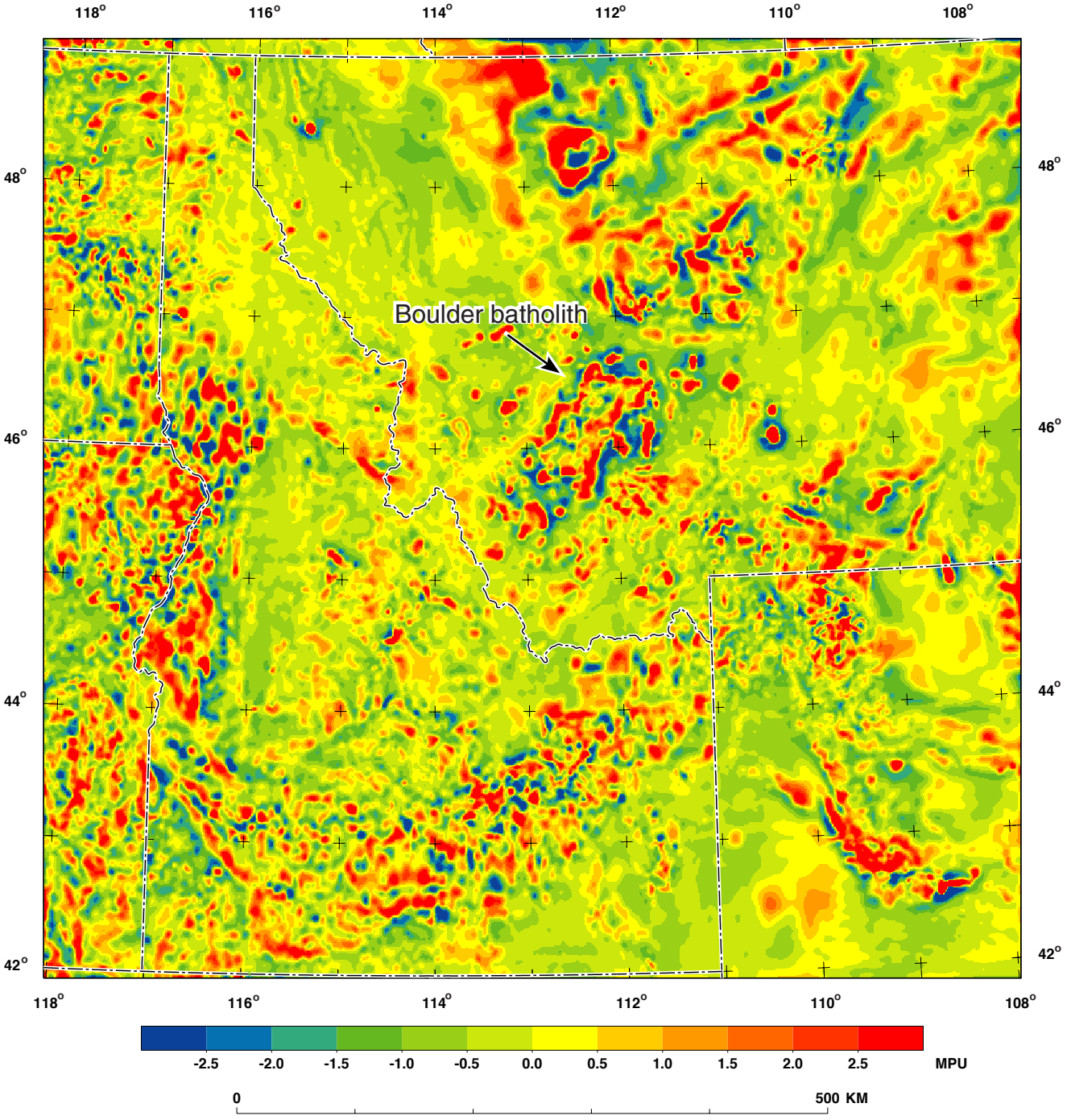

Figure 17. Intermediate-wavelength magnetic potential. A matched filter was applied to the magnetic potential of figure 15 to enhance magnetic sources in the upper crust.

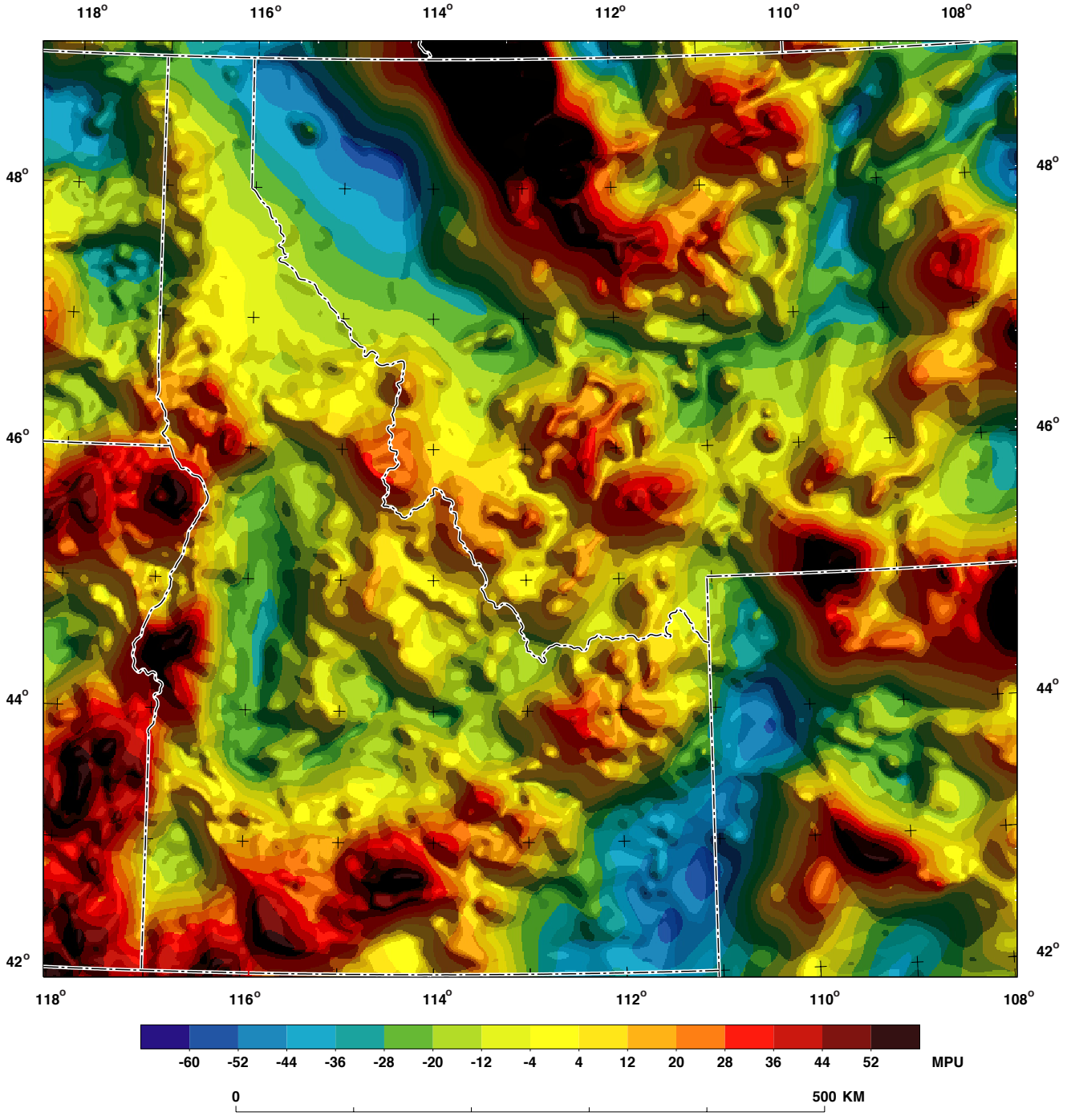

Figure 18. Long-wavelength magnetic potential. A matched filter was applied to the magnetic potential of figure 15 to enhance magnetic sources in the middle to upper crust.

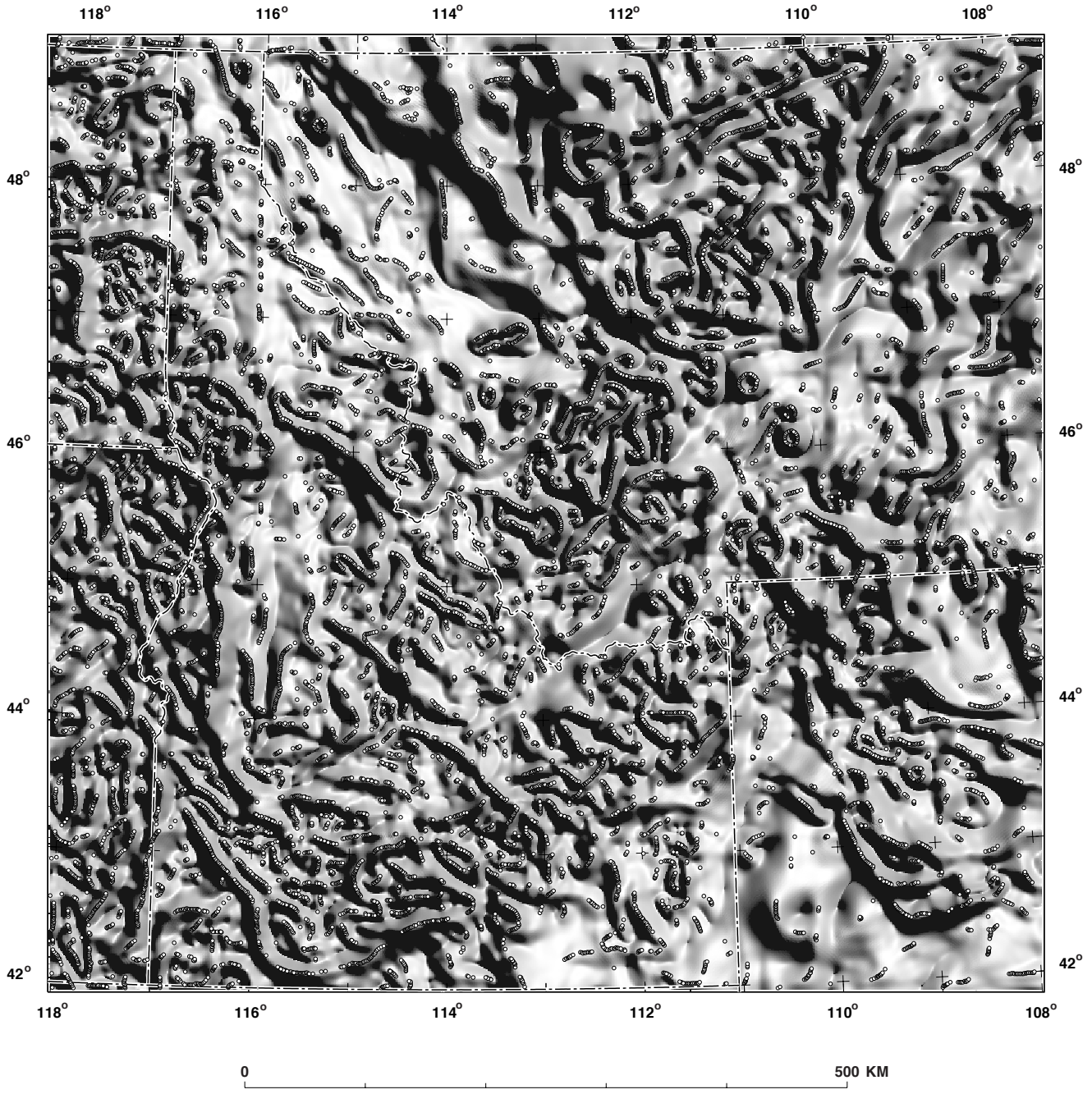

Figure 19. Shaded-relief map of horizontal gradients in the long-wavelength magnetic potential data shown in figure 18. Open circles are maximum values of these gradients calculated using the method of Blakely and Simpson (1986).

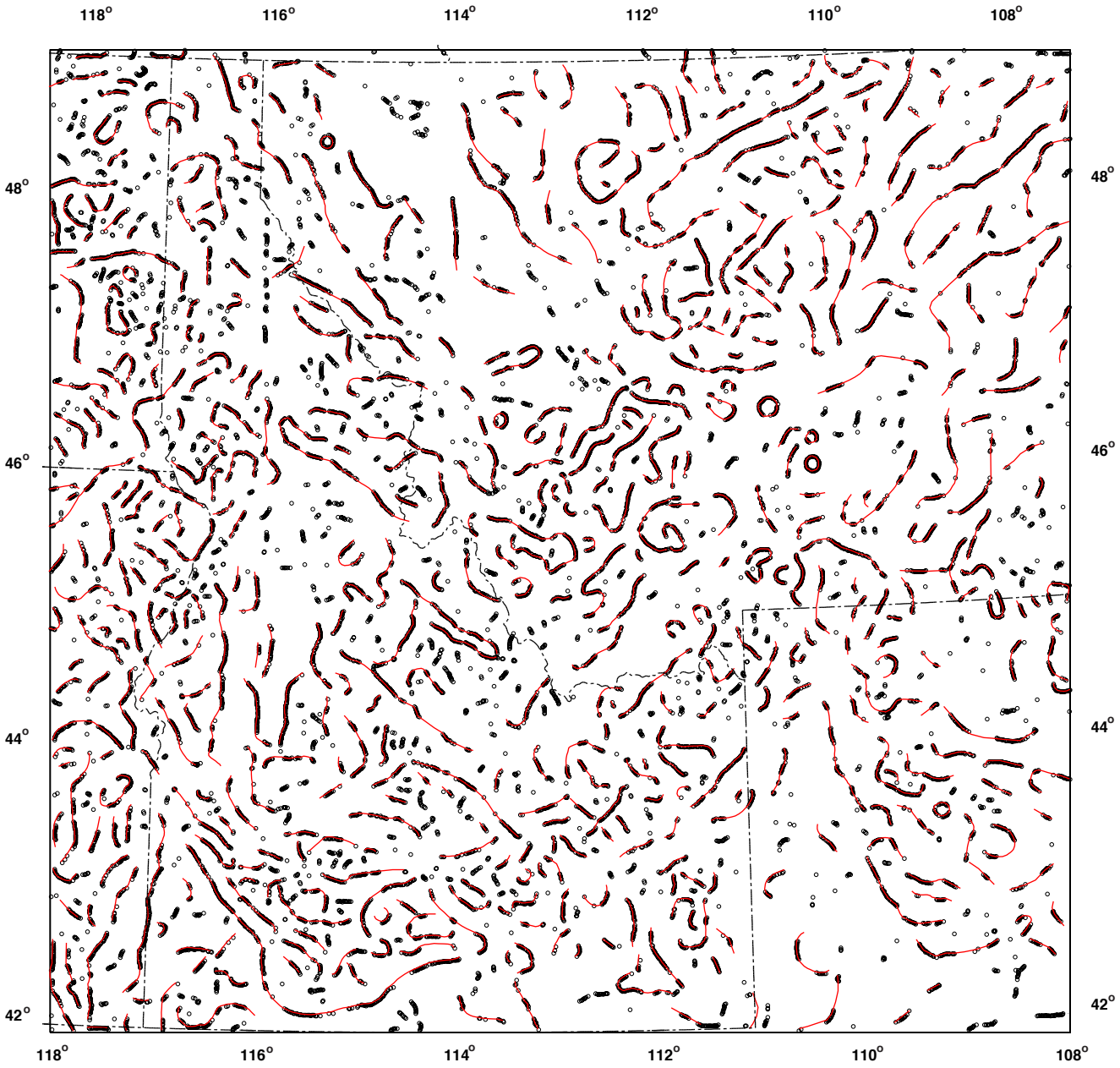

Figure 20. Interpreted major magnetization boundaries (red lines) within the middle to upper crust constrained by maxima in the horizontal gradients shown in figure 19.